IDENTIFICATION OF THE CURRENT DISTRIBUTION ON A RADOME FROM NEAR-FIELD MEASUREMENTS

K. Persson[1], **M. Gustafsson**[2], **M. Andersson**[3]

[1] ***Department of Electroscience, Electromagnetic Theory, Lund Institute of Technology, Box 118 S-221 00 Lund, Sweden, email: f96kp@es.lth.se***

[2] ***As (1) above, but email: mats@es.lth.se***

[3] ***Applied Composites AB, Box 163, 341 23 Ljungby, Sweden, email: michael.andersson@acab.se***

ABSTRACT

Information about the equivalent current distribution on a radome can be used to improve radome design, detect manufacturing errors, and to verify numerical simulations. In this paper, the transformation from near-field data to the equivalent current distribution is analyzed. The transformation is based on a singular value decomposition of the surface integral equation that relates the equivalent current to the near-field data. The attempt is to develop a mathematical model that easily can be used for arbitrary geometric structures. The symmetries of a specific problem is used to reduce the computational complexity. Both synthetic data and measured data are used to verify the algorithm.

1 INTRODUCTION

There are several applications of a near field to equivalent current transformation. For example, if the radiation pattern from a radiating body (radome, antenna array) does not exhibit the expected form. One can determine the equivalent current on the radiating body and directly find the malfunctioning components instead of dismounting the radiating body and looking for defect components. Another application is in the radome industry where computer simulations are used to analyze radome structures. These simulations need input data depicting the field from the antenna placed inside the radome in an accurate way. A person not initiated in this area might wonder why one cannot simply measure the field from the antenna at the distances where the radome should be placed. The reason for this is that the radome often is placed very close to the antenna and at these distances, there is a substantial interaction between the antenna and the measuring probe [1, 2, 3].

In this paper, the transform of near-field data to its equivalent current distribution on a surface close to the radiating body is analyzed. This transformation is a linear inverse source problem. As most inverse problems it is ill posed, *i.e.*, small errors in the near-field data can produce large errors in the equivalent current. The surface integral representation of the electric field is used to construct the inversion algorithm [3, 4]. This gives an integral equation in the unknown electric and magnetic currents on the radome surface and the measured electric field. An additional integral equation is given by the fact that the equivalent current is constructed such that the field is zero inside the radome surface, *i.e.*, the extinction theorem [5]. The integral equation is discretized by local base functions to give a matrix equation. To reduce the computational complexity rotational symmetric structures are considered. In this case, a fast Fourier transform can be used to diagonalize the rotational part of the problem, *i.e.*, the original surface-to-surface linear map is decomposed into a set of line-to-line linear maps. A singular value decomposition (SVD) is used invert each of these linear maps. The problem is regularized by suppression of small singular values in the inversion. In this paper, the field is presumed to be scalar. This assumption is acceptable since the measured near-field data clearly have one dominating component.

2 RADOME EXAMPLE

The used near-field data is supplied by SAAB Bofors Dynamics and Applied Composites AB (ACAB), Sweden, see Fig. 1. The measured electric field has a dominating z-component. Three different measurements are done, data sampled without the radome, data sampled with the radome, and data sampled with the defect radome. The defect radome is constructed by attaching two copper plates on the radome surface. The setup with relevant dimensions indicated are depicted in Fig. 1. The antenna is a reflector antenna with the diameter $0.32\,\mathrm{m}$ and a focal distance of $0.1\,\mathrm{m}$. It is vertically polarized relative to the horizontal plane. The standing wave ratio is 1.4 in the frequency range $8 - 9.5\,\mathrm{GHz}$. The antenna is poorly adapted for other frequencies. A $10\,\mathrm{dB}$ reflection attenuator is connected to the antenna. The radome surface is described by $\rho(z) = z_0$ for $z_1 \leq z \leq z_2$ and

$$\rho(z) = -(bz' + d) + \sqrt{(bz' + d)^2 - a(z')^2 - 2cz' - e} \quad \text{for } z_2 < z \leq z_3 \text{ where } z' = z - z_1$$

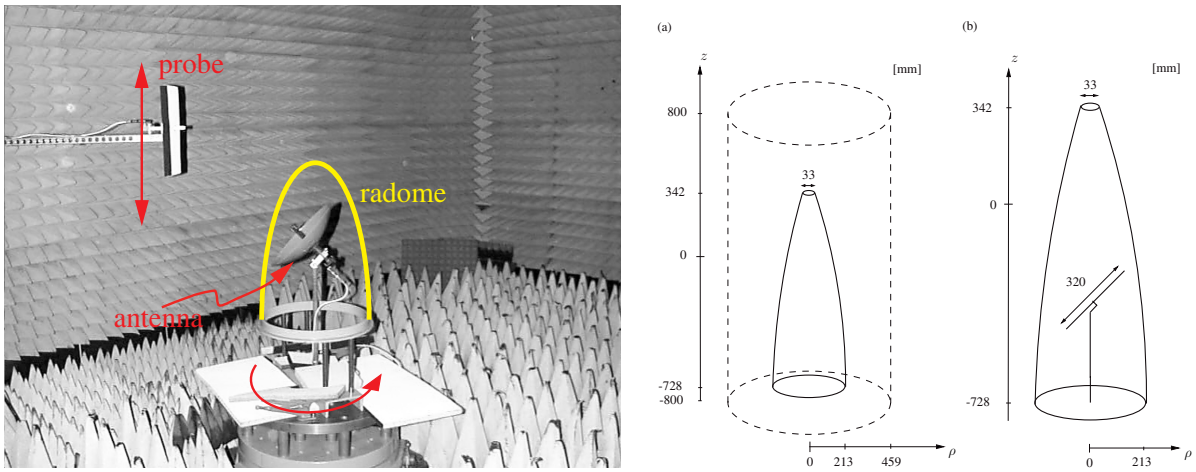

Fig. 1. Photo of the cylindrical near-field range at SAAB Bofors Dynamics, Sweden. (By courtesy of SAAB Bofors Dynamics and Applied Composites AB, Sweden.) (a) The dimensions of the radome and the cylindrical surface where the near field is measured. (b) The dimensions of the radome and the reflector antenna.

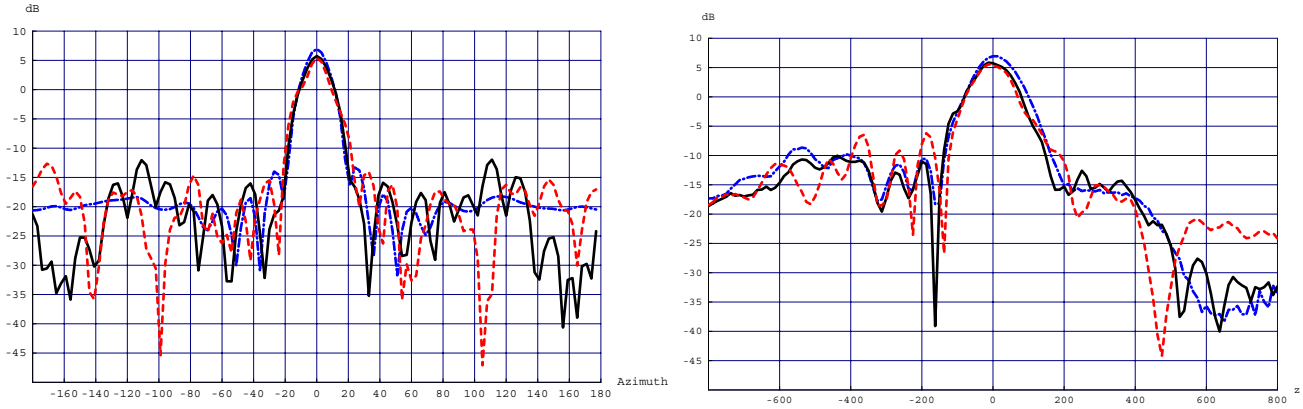

Fig. 2. Example of the measured field in the angular ($z = 0$) and hight ($\phi = 0$) directions, respectively. The solid, dashed, and point dashed lines correspond to the measurements with the radome, with the defect radome, and without the radome, respectively.

and the constants are $a = 0.122$, $b = 0.0483$, $c = -0.018\,\mathrm{m}$, $d = 0.148\,\mathrm{m}$, $e = -0.108\,\mathrm{m}^2$, $z_1 = -0.728\,\mathrm{m}$, $z_2 = -0.663\,\mathrm{m}$, and $z_3 = 0.342\,\mathrm{m}$. The near-field probe consists of a waveguide for which no compensation is made in the final data [1]. The cylinder surface, where the field is sampled, is placed in both the reactive near-field zone and the radiating near-field zone [6]. In this way the coupling between the measuring near-field probe and the object is reduced.

The amplitude and phase of the electric field are measured in the frequency range $8 - 9.5\,\mathrm{GHz}$. The electric field is sampled on a cylindrical surface by moving the probe in the z-direction and rotating the antenna under test, see Fig. 1. Angle wise, 120 points is measured going from $-180°$ to $180°$ in steps of $3°$. The z-dimension is divided into 129 points, each separated by $12.5\,\mathrm{mm}$. This means that at $8\,\mathrm{GHz}$ the field is sampled three times per wavelength. Together, a total of $120 \cdot 129 = 15480$ measuring points are sampled for each setup and frequency. Example of the field amplitude as a function of the angle and hight, respectively, is shown in Fig. 2.

3 THE SURFACE INTEGRAL REPRESENTATION

The scalar surface integral representation (SIR)

$$\iint_{\text{radome}} \frac{\partial g(k,\boldsymbol{r},\boldsymbol{r}')}{\partial n} E_z(\boldsymbol{r}) - g(k,\boldsymbol{r},\boldsymbol{r}') \frac{\partial E_z(\boldsymbol{r})}{\partial n}\,\mathrm{dS} = \begin{cases} -E_z(\boldsymbol{r}') & \boldsymbol{r}' \in V \\ 0 & \boldsymbol{r}' \notin V \end{cases} \tag{3.1}$$

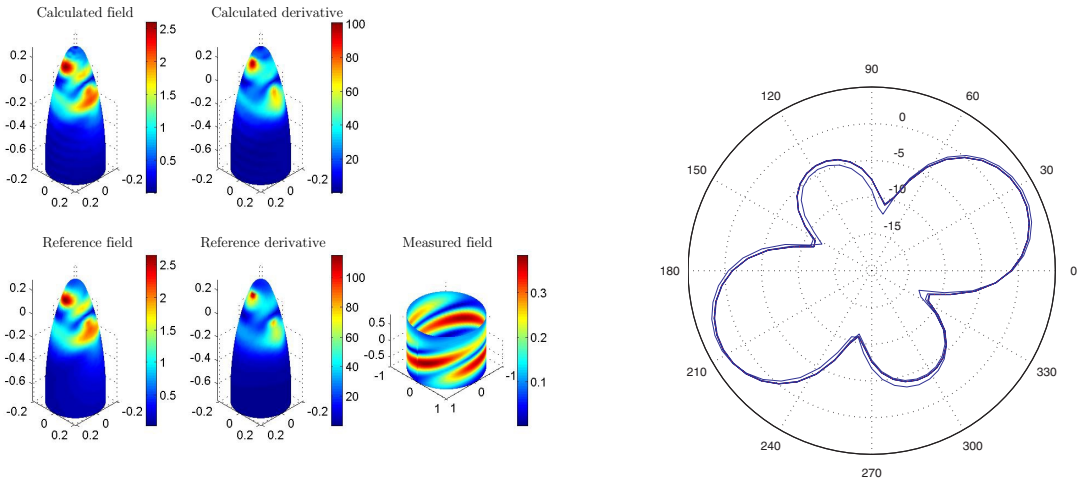

Fig. 3. Synthetic data originating from five point sources inside the radome. The data is reversed to its equivalent current on the radome surface. The frequency is 1.7 GHz and the cut-off value is $\delta = 10^{-8}$. The number of sample points per wavelength are 6.7 in the angular direction and 7.7 in the z-direction. Far-field pattern (for the spherical coordinates $\theta = 90^\circ$ and $0 < \phi < 360^\circ$) from the equivalent current distribution, depicted for the different cut-off values shown in Fig. 4.

is used to relate the field on the radome surface to the measured field. Observe that the true electric field does not have to be zero outside the volume. The SIR (3.1) only says that the lefthandside of the equation turns out to be zero if the vector $\boldsymbol{r}'$ points outside the volume V.

The equivalent surface currents are introduced as $M(\boldsymbol{r}) = E_z(\boldsymbol{r})$ and $J(\boldsymbol{r}) = \frac{\partial E_z(\boldsymbol{r})}{\partial n}$. These designations are not in total accordance with the actual definitions of the electric and magnetic equivalent currents which are $\boldsymbol{M}(\boldsymbol{r}) = -\hat{\boldsymbol{n}}\times\boldsymbol{E}(\boldsymbol{r})$ and $\boldsymbol{J}(\boldsymbol{r}) = \hat{\boldsymbol{n}}\times\boldsymbol{H}(\boldsymbol{r})$, see also [5]. Even so, the similarities with the quantities in (3.1) make them plausible designations for the purposes of this paper. Bear also in mind that these denominations are not true currents. The equivalent currents M and J are only a way of describing the electromagnetic field so that the field in the volume enclosed by the surface at which the current exists can be set to zero.

The transformation (Green's function) is rotational symmetric since the measurement setup is rotational symmetric. This reduces (3.1) to an angle wise convolution which makes it possible to evaluate the SIR by an angle wise Fourier transform

$$\sum_m \hat{G}_{i,m,k_j} \begin{pmatrix} \hat{M}_{m,k_j} \\ \hat{J}_{m,k_j} \end{pmatrix} = \frac{1}{N} \begin{pmatrix} -\hat{E}^{\mathrm{cyl}}_{i,k_j} \\ 0 \end{pmatrix} \quad \text{for all } i, j. \tag{3.2}$$

Since the matrix $\hat{G}$ in (3.2) is not quadratic a regular inversion can not be done. A fast and easy way to solve this is to use the singular value decomposition (SVD), see [7]. The matrix $\hat{G}$ can by this method be divided into three matrices so that $\hat{G} = \hat{U}\hat{S}\hat{V}'$ where $\hat{U}$ and $\hat{V}'$ are orthogonal matrices, *i.e.*, $\hat{U}^{-1} = \hat{U}'$ and $\hat{V}^{-1} = \hat{V}'$ where $\hat{V}'$ denotes the Hermitian conjugate of $\hat{V}$. A cut-off value δ is chosen and all singular values below this value are set to zero. If this is not done the small singular values will create tremendously growth of non-radiation currents.

4 INVERSION RESULTS WITH SYNTHETIC DATA

The inversion algorithm is implemented in MATLAB. One of the major computational problems is due to the storage of the matrix G, *i.e.*, G has approximately 10^8 elements. To verify the computer code a rather low frequency is used to reduce the amount of necessary sample points and hence the memory requirement. For a frequency of 1.7 GHz a sample density of 15.7 points per wavelength in the angular direction and 15.9 points in the z-direction can easily be attained. For easier calculations the radome surface is reshaped in a continuous way, where a smooth top and bottom surface have been added to the radome. The synthetic data is calculated from five point sources placed inside the radome. The inversion result and the corresponding far field pattern are shown in Fig. 3.

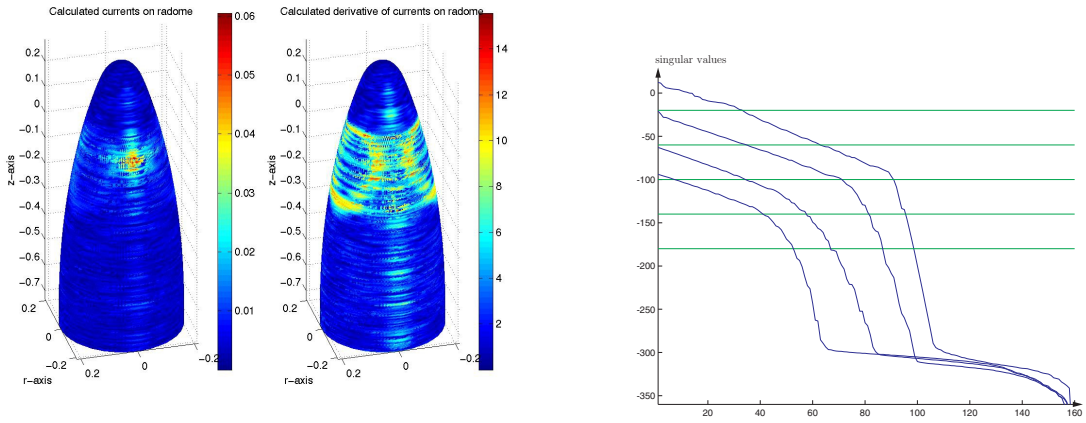

Fig. 4. Measured data reversed to its equivalent current at the radome surface. The frequency is $8\,\mathrm{GHz}$ and the cut-off value is 1. The number of sample points per wavelength are 6.7 in the angular direction and 10.2 in the z-direction. The singular values of $\hat{G}$ in dB scale for four of the Fourier transformed angle components. The horizontal lines show different cut-off values.

5 INVERSION RESULTS WITH EXPERIMENTAL DATA

Inversion with the measured near-field data, described in Section 2, is shown in Fig. 4. The results are preliminary and more analysis is needed before the results become reliable. To be able to rule out errors originating from a low sample density, the inversion results are compared the results with synthetic data. Another source of error are reflections in the measured data from the walls and floors surrounding the radome.

6 CONCLUSIONS

The used surface integral representation gives a linear map between the equivalent current and the near-field data for general structures. It is shown that this map can be inverted for rotational symmetric geometries. The inversion results for synthetic data are very good. The preliminary inversion results for the measured data are promising but more analysis is needed in this case. The good results for this scalar approximation is also very promising for a full vector implementation of the near field to equivalent current transformation.

7 ACKNOWLEDGMENT

SAAB Bofors Dynamics and Applied Composites AB (ACAB), Sweden are gratefully acknowledged for supplying the experimental data and the photo in Fig. 1.

REFERENCES

[1] J. E. Hansen, ed. *Spherical Near-Field Antenna Measurements*. No. 26 in IEE electromagnetic waves series. Stevenage, UK: Peter Peregrinus Ltd., 1988. ISBN: 0-86341-110-X.

[2] A. D. Yaghjian. “An overview of near-field antenna measurements”. *IEEE Trans. Antennas Propagat.*, vol. 34(1), pp. 30–45, Jan. 1986.

[3] Y. Rahmat-Samii, L. I. Williams, and R. G. Yaccarino. “The UCLA bi-polar planar-near-field antenna-measurement and diagnostics range”. *jou-IEEE-APMag*, vol. 37(6), pp. 16–35, Dec. 1995.

[4] T. K. Sarkar and A. Taaghol. “Near-field to near/far-field transformation for arbitrary near-field geometry utilizing an equivalent electric current and MoM”. *IEEE Trans. Antennas Propagat.*, vol. 47(3), pp. 566–573, Mar. 1999.

[5] C. A. Balanis. *Advanced Engineering Electromagnetics*. New York: John Wiley & Sons, 1989.

[6] C. A. Balanis. *Antenna Theory*. New York: John Wiley & Sons, 2nd edn., 1997.

[7] G. Strang. *Introduction to applied mathematics*. Box 157, Wellesley MA 02181: Wellesley-Cambridge Press, 1986.